Lop-sided diffractions of distinct symmetries in 2D non-Hermitian optical gratings

Yi-Mou Liu,[1] Feng Gao,[2] Jin-Hui Wu,[1,*] M. Artoni,[3] and G. C. La Rocca[4]

[1]*School of Physics, Northeast Normal University, Changchun 130024, China*
[2]*College of Physics, Jilin University, Changchun 130012, China*
[3]*Department of Engineering and Information Technology and Istituto Nazionale di Ottica (INO-CNR), Brescia University, 25133 Brescia, Italy*
[4]*Scuola Normale Superiore and CNISM, 56126 Pisa, Italy*

(Dated: July 30, 2019)

Fraunhofer light diffraction across a thin 2D lattice of cold atoms subject to transverse hybrid modulations of two standing-wave crossed pump fields is seen to yield lop-sided patterns of various degrees of symmetry. We show that one can fully restrain the diffraction of a weak incident probe to two diagonal or adjacent quadrants or even just to a single quadrant, depending on the phases of two standing-wave pumps and on the probe detuning. Different diffraction symmetries with respect to the axes or diagonals of the diffraction plane quadrants are here interpreted in terms of different out-of-phase interplay of absorption and dispersion periodic distributions, resulting from different combinations of Hermitian, $\mathcal{PT}$-symmetric, and non-Hermitian modulations.

I. INTRODUCTION

Non-Hermitian optical systems with parity-time ($\mathcal{PT}$) symmetry [1–4] and antisymmetry [5–9] have attracted a great deal of attention because they provide new possibilities for controlling photon flows with various interesting characteristics. Optical $\mathcal{PT}$ symmetry typically requires the complex refractive index to satisfy the condition $n(x) = n^*(-x)$ in a given direction. As opposed to $\mathcal{PT}$ symmetry, $\mathcal{PT}$ antisymmetry is realized in optical media with the complex refractive index satisfying instead the condition $n(x) = -n^*(-x)$. Recent work has reported that $\mathcal{PT}$ symmetry and antisymmetry can simultaneously occur in the same optical structure [10–12], whereas feasible ways to convert from one to the other are discussed in [8, 9]. More importantly, non-Hermitian optical structures have been explored to extend fascinating studies on optical Bloch oscillation [13, 14], coherent perfect absorption [15], photon or phonon lasing [16-19], etc; have become the basis of a few nonreciprocal optical phenomena like unidirectional reflection [20, 21], unidirectional invisibility [22, 23], and asymmetric diffraction [24–26]. In addition, complex crystals described by a non-Hermitian Hamiltonian with a complex periodic potential are expected to host important spectral singularities whose signatures may be assessed through a typical Bragg diffraction experiment [27].

Applying standing-wave (SW), instead of traveling-wave (TW), control fields in the atomic media subject to electromagnetically induced transparency (EIT) [28–34], is an efficient way for realizing complex periodic potentials that lay at the basis of well known phenomena such as dynamically tunable photonic bandgaps (PBGs) [35–37] and stationary light pulses (SLPs) [38–40]. This method has also been used to realize structures of electromagnetically induced gratings (EIGs) [41–44] with special forms of spatially periodic absorption and dispersion. One main advantage of such Hermitian EIG structures is that intensity distributions of the diffracted photons among different orders can be manipulated "on demand" through flexible amplitude and/or phase modulations of the transmission function. This may be explored to generalize earlier works on lop-sided diffraction of atomic (optical) waves off 1D non-Hermitian optical (atomic) gratings with fixed potentials [45, 46]. In fact, unconventional optical modulations on EIG structures have recently brought to the development of cooperative nonlinear gratings and non-Hermitian gratings. Cooperative nonlinear gratings allow one to distinguish light fields of different photon statistics with the dipole blockade effect of Rydberg atoms [47, 48], while non-Hermitian gratings typically result in asymmetric diffraction patterns that can be tuned through the out-of-phase interplay of phase and amplitude modulations [49–52]. Unidirectional and controlled higher-order diffraction, through non-Hermitian modulations on EIG structures built from Rydberg atoms driven beyond the dipole blockade regime, has also been reported [53]. Most of above works hinge, however, on one-dimensional (1D) Hermitian or non-Hermitian EIG structures.

We investigate here instead a two-dimensional (2D) non-Hermitian EIG structure consisting of a square optical lattice filled with ultracold atoms driven into the four-level $\mathcal{N}$ configuration [see Fig. 1] by two TW pumps and two orthogonal SW pumps (*2D pump cross-gratings*) [see Fig. 2(a)]. This realizes a thin 2D non-Hermitian grating that, under specific driving conditions, enable one to attain an arbitrary combination of Hermitian, $\mathcal{PT}$-symmetry, and non-Hermitian modulations on the probe absorption and dispersion along the two orthogonal lattice axes. Such modulations, which may be "pure" or "hybrid", result in peculiar diffraction patterns bearing *double diagonal, single axial, and single diagonal* symme-

*Electronic address: jhwu@nenu.edu.cn

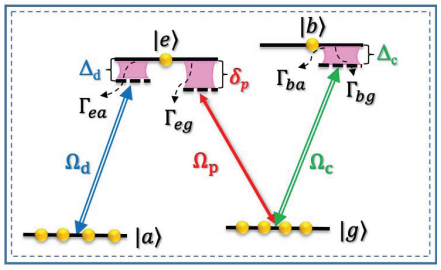

FIG. 1: A four-level $\mathcal{N}$ configuration for ^{87}Rb atoms driven by a probe field of Rabi frequency (detuning) Ω_p (δ_p) and two pump fields of Rabi frequencies (detunings) Ω_d and Ω_c (Δ_d and Δ_c). The four levels are $|g\rangle \equiv |5S_{1/2}, F = 1\rangle$, $|a\rangle \equiv |5S_{1/2}, F = 2\rangle$, $|e\rangle \equiv |5P_{1/2}, F = 1\rangle$, and $|b\rangle \equiv |5P_{1/2}, F = 2\rangle$ with decay rates $\Gamma_{eg} = \Gamma_{bg} = \Gamma_{ea} = \Gamma_{ba} \simeq 2\pi \times 5.9$ MHz.

tries in the diffraction plane. Consequently, we observe diffracted photons only in two diagonal quadrants, two adjacent quadrants, or a single quadrant while diffraction patterns can be made to undergo a $\pi/2$-rotation sweep by just changing the probe detuning and/or the pump phases. It is finally worth mentioning that the lop-sided diffraction mechanism we propose here may turn out to be relevant to the development of new concepts on wavefront shaping that are now attained instead through metasurfaces with subwavelength resolutions [54–56].

This work is organized through the following sect. II, where we summarize the background model, and sect. III where we discuss the far-field Fraunhofer diffraction resulting from three types of pure or hybrid modulations and interpret the results as arising from the out-of-phase interplay between real (dispersion) and imaginary (absorption) parts of the probe susceptibility. We summarize at last our conclusions in sect. IV.

II. THE MODEL.

We start by considering the four-level $\mathcal{N}$ configuration of cold ^{87}Rb atoms driven by three coherent fields of frequencies (amplitudes) ω_p ($\mathcal{E}_p$), ω_c ($\mathcal{E}_c$) and ω_d ($\mathcal{E}_d$) as shown in Fig. 1. The weak probe field ω_p interacts with transition $|g\rangle \leftrightarrow |e\rangle$, while the strong pump fields ω_c and ω_d act upon transitions $|g\rangle \leftrightarrow |b\rangle$ and $|a\rangle \leftrightarrow |e\rangle$, respectively. The corresponding detunings (Rabi frequencies) are defined as $\delta_p = \omega_p - \omega_{eg}$ ($\Omega_p = \mathcal{E}_p \cdot \wp_{ge}/\hbar$), $\Delta_c = \omega_c - \omega_{bg}$ ($\Omega_c = \mathcal{E}_c \cdot \wp_{gb}/\hbar$), and $\Delta_d = \omega_d - \omega_{ea}$ ($\Omega_d = \mathcal{E}_d \cdot \wp_{ae}/\hbar$) with ω_{ij} being transition frequencies and $\wp_{ij}$ dipole moments. The atoms are assumed to be loaded into a square optical lattice of period a along both x and y axes [see Fig. 2(a)]. Around the intensity maxima formed by two (Gaussian) counter-propagating red-detuned laser beams, a depth minimum occurs leading to an approximately *harmonic* lattice potential trap [57, 58]. Assuming that (*i.*) all lattice traps are equally populated and (*ii.*) the trapped atoms are cool enough to occupy the lowest energy levels, we represent the atomic density distribution at each (trap) site $\{x_i, y_i\}$ as

$$N_{i,j}(x,y) = N_0 e^{-[(x-x_i)^2/\sigma_x^2 + (y-y_j)^2/\sigma_y^2]} \quad (1)$$

corresponding to the ground state of a 2D (harmonic) trap [59]. Here N_0 is the (average) peak density while σ_x and σ_y are the (average) half widths of a Gaussian distribution along the transverse trapping directions [60]. The above assumptions enable us to introduce the periodic susceptibility exhibited by the incident probe

$$\chi_p(x,y) = \frac{\wp_{ge}^2}{2\varepsilon_0 \hbar \Omega_p} \sigma_{ge} \sum_{i,j} N_{i,j}(x,y) = \alpha \sigma_{ge} N(x,y) \quad (2)$$

with $\alpha = \wp_{ge}^2/2\varepsilon_0\hbar\Omega_p$. The polarization σ_{ge} can be obtained by solving the density matrix equations

$$\begin{aligned}
\partial_t \sigma_{gg} &= \Gamma_{bg}\sigma_{bb} + \Gamma_{eg}\sigma_{ee} + i\Omega_c^*\sigma_{bg} - i\Omega_c\sigma_{gb} + i\Omega_p^*\sigma_{eg} - i\Omega_p\sigma_{ge},\\
\partial_t \sigma_{aa} &= \Gamma_{ba}\sigma_{bb} + \Gamma_{ea}\sigma_{ee} + i\Omega_d^*\sigma_{ea} - i\Omega_d\sigma_{ae},\\
\partial_t \sigma_{bb} &= -\Gamma_{ba}\sigma_{bb} - \Gamma_{bg}\sigma_{bb} + i\Omega_c\sigma_{gb} - i\Omega_c^*\sigma_{bg},\\
\partial_t \sigma_{ga} &= -\gamma'_{ga}\sigma_{ga} + i\Omega_c^*\sigma_{ba} + i\Omega_p^*\sigma_{ea} - i\Omega_d\sigma_{ge},\\
\partial_t \sigma_{gb} &= -\gamma'_{gb}\sigma_{gb} + i\Omega_c^*\sigma_{eb} + i\Omega_c^*(\sigma_{bb} - \sigma_{gg}),\\
\partial_t \sigma_{ge} &= -\gamma'_{ge}\sigma_{ge} + i\Omega_c^*\sigma_{be} + i\Omega_p^*(\sigma_{ee} - \sigma_{gg}) - i\Omega_d^*\sigma_{ga},\\
\partial_t \sigma_{ab} &= -\gamma'_{ab}\sigma_{ab} + i\Omega_d^*\sigma_{eb} - i\Omega_c^*\sigma_{ag},\\
\partial_t \sigma_{ae} &= -\gamma'_{ae}\sigma_{ae} - i\Omega_p^*\sigma_{ag} + i\Omega_d^*(\sigma_{ee} - \sigma_{aa}),\\
\partial_t \sigma_{be} &= -\gamma'_{be}\sigma_{be} + i\Omega_c\sigma_{ge} - i\Omega_p^*\sigma_{bg} - i\Omega_d^*\sigma_{ba},
\end{aligned} \quad (3)$$

that arise as usual from the interaction Hamiltonian, in the rotating-wave & electric-dipole approximations, associated with our $\mathcal{N}$-type driving configuration

$$\begin{aligned}
\mathcal{H}_I = \hbar[&\delta_p\hat{\sigma}_{ee} + (\delta_p - \Delta_d)\hat{\sigma}_{aa} + \Delta_c\hat{\sigma}_{bb}\\
&+ \hbar[\Omega_p\hat{\sigma}_{eg} + \Omega_d\hat{\sigma}_{ea} + \Omega_c\hat{\sigma}_{bg} + h.c.].
\end{aligned} \quad (4)$$

Here $\hat{\sigma}_{\mu\nu} = |\mu\rangle\langle\nu|$ define the projection ($\mu = \nu$) and transition ($\mu \neq \nu$) operators [61] and their expectation values $\sigma_{\mu\mu}$ and $\sigma_{\mu\nu}$ denote atomic population at level $|\mu\rangle$ and atomic coherence between levels $|\mu\rangle$ and $|\nu\rangle$, respectively. They satisfy the properties $\sum_\mu \sigma_{\mu\mu} = 1$ and $\sigma_{\mu\nu} = \sigma_{\nu\mu}^*$ while $\gamma_{\mu\nu} = \sum_k(\Gamma_{\mu k} + \Gamma_{\nu k})/2$ denote the dephasing rates with Γ_{eg} and Γ_{ea} (Γ_{bg} and Γ_{ba}) being the decay rates from level $|e\rangle$ ($|b\rangle$) to levels $|g\rangle$ and $|a\rangle$, respectively. We also introduce the multi-photon detunings $\Delta_{ga} = \delta_p - \delta_d$, $\Delta_{be} = \delta_p - \delta_c$, and $\Delta_{ab} = \delta_c + \delta_d - \delta_p$ as well as the complex dephasing rates $\gamma'_{ga} = \gamma_{ga} + i\Delta_{ga}$, $\gamma'_{gb} = \gamma_{gb} + i\delta_c$, $\gamma'_{ge} = \gamma_{ge} + i\delta_p$, $\gamma'_{ab} = \gamma_{ab} + i\Delta_{ab}$, $\gamma'_{ae} = \gamma_{ae} + i\delta_d$, and $\gamma'_{be} = \gamma_{be} + i\Delta_{be}$ for convenience in Eq. (3).

The real $\chi_p^R(x,y)$ and imaginary $\chi_p^I(x,y)$ parts in Eq. (2) describe the probe *dispersion* and *absorption* properties, respectively. When $\Omega_{c,d}$ and $\delta_{c,d}$ are "constant", changes of $\chi_p^R(x,y)$ and $\chi_p^I(x,y)$ along both x and y axes occur "in-phase". This would lead to a *traditional* 2D EIG

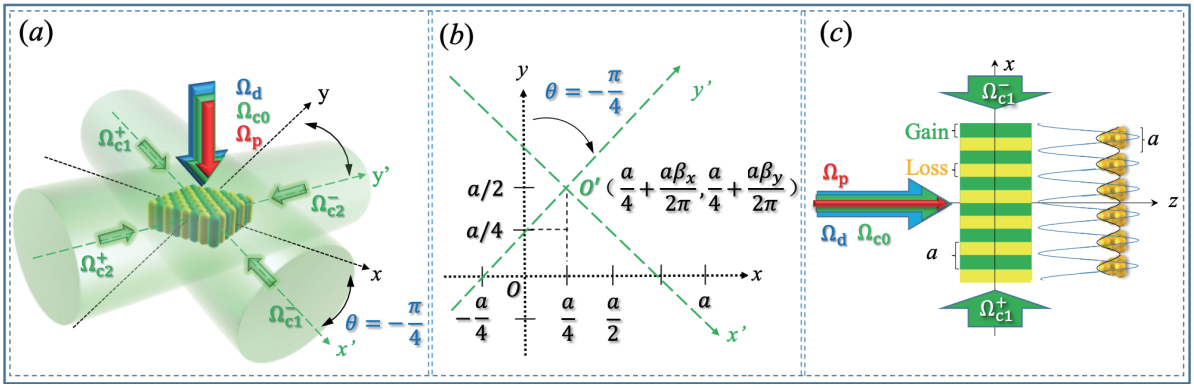

FIG. 2: (a) Non-Hermitian 2D pump grating along the x' and y' axes (period $a/\sqrt{2}$) modulating a 2D atomic lattice along the x and y axes (period a) with Ω_{c0}, $\Omega_{c1}^{\pm}$, and $\Omega_{c2}^{\pm}$ together taking the role of Ω_c in Fig. 1. (b) Details on the $O(x,y)$ and $O'(x',y')$ coordinate systems of relative orientations given in terms of their origins and axes. (c) A side view of the 2D grating, *i.e.*, its projection in the xz plane with balanced gain (*green*) and loss (*yellow*) in the $\mathcal{PT}$-symmetry regime.

structure exhibiting the symmetric diffraction patterns [62, 63]. However, *nontrivial* 2D EIG structures may be attained if changes of $\chi_p^R(x,y)$ and $\chi_p^I(x,y)$ along the x and/or y axes can be set to occur "not-in-phase", *e.g.*, through the following crossed-pump modulation,

$$\begin{aligned}\Omega_c(x,y) &= \Omega_{c0}+\Omega_{c1}(x')+\Omega_{c2}(y')=\Omega_{c0}+\frac{1}{2}\delta\Omega_c\cos\frac{x'}{a/2\sqrt{2}\pi}+\frac{1}{2}\delta\Omega_c\cos\frac{y'}{a/2\sqrt{2}\pi}\\ &= \Omega_{c0}+\frac{1}{2}\delta\Omega_c\cos\frac{(x-\delta x)-(y-\delta y)}{a/2\pi}+\frac{1}{2}\delta\Omega_c\cos\frac{(x-\delta x)+(y-\delta y)}{a/2\pi}\\ &= \Omega_{c0}+\delta\Omega_c\cos\frac{(x-\delta x)}{a/2\pi}\cos\frac{(y-\delta y)}{a/2\pi}=\Omega_{c0}+\delta\Omega_c\cdot f(x,y).\end{aligned} \tag{5}$$

Here $(\delta x,\ \delta y)$ denote the amounts by which the maxima of Rabi frequency $\Omega_c(x,y)$ shift relative to the corresponding maxima of density distribution $N(x,y)$. We denote by Ω_{c0} a constant TW component while $\Omega_{c1}(x')$ and $\Omega_{c2}(y')$ are two SW components of period $a/\sqrt{2}$ along the two orthogonal axes x' and y' rotated by an angle $\theta=-\pi/4$ relative to the xy plane [see Figs. 2(a) and 2(b)]. For convenience in the following discussion, we further rewrite the modulating factor as

$$f(x,y)=\sin\left(\frac{x}{a/2\pi}-\beta_x\right)\sin\left(\frac{y}{a/2\pi}-\beta_y\right) \tag{6}$$

by rescaling $\delta x=a/4+a\beta_x/2\pi$ and $\delta y=a/4+a\beta_y/2\pi$. The off-center cross modulation in Eqs. (5-6) thus results in a space-dependent probe coherence $\sigma_{ge}(x,y)$ which, together with $N(x,y)$ in Eq. (2), yields *nontrivial* modulations on our atomic lattice whose diffraction features will be discussed in the next section. A side view of the 2D lattice under the $\mathcal{PT}$-symmetry modulation has been shown in Fig. 2(c) to gain a clearer impression.

For a weak probe impinging perpendicular to the 2D atomic lattice shown in Fig. 2(a), the (far-field) diffraction intensity [62, 63] can be written in the *thin scatterer approximation* [64] as

$$I_p(\theta_x,\theta_y)\approx\left|E_p^I(\theta_x,\theta_y)\right|^2\cdot\left[\frac{\sin(\pi MR\sin\theta_x)}{M\sin(\pi R\sin\theta_x)}\cdot\frac{\sin(\pi MR\sin\theta_y)}{M\sin(\pi R\sin\theta_y)}\right]^2, \tag{7}$$

where the geometric factors depend on two ratios $R=a/\lambda_p$ and $M=w_o/a$, with w_o being the width of the incident probe beam. We have also denoted by θ_x and

θ_y the diffraction angles with respect to the z direction in the xz and yz planes. More specifically, probe diffraction will take place in a few directions determined by the diffraction order $\{m, n\}$ according to angles $\theta_x \to \theta_{x,m} = \arcsin(m/R)$ and $\theta_y \to \theta_{y,n} = \arcsin(n/R)$, the number of diffraction orders depending on the ratio R. The single square lattice (*i.e.*, 2D unit cell) diffraction function

$$E_p^I(\theta_x, \theta_y) = \int_{-\frac{a}{2}}^{\frac{a}{2}} \int_{-\frac{a}{2}}^{\frac{a}{2}} T_L(x, y) e^{-i2\pi R(x \sin\theta_x + y \sin\theta_y)} dx dy, \tag{8}$$

depends instead on the probe dispersion and absorption directly through the transmission

$$T_L(x, y) = e^{-2\pi L \chi_p^I(x,y)/\lambda_p} \cdot e^{i2\pi L \chi_p^R(x,y)/\lambda_p} \tag{9}$$

across a short distance L in the z direction [65, 66]. Note that *phase* and *amplitude* modulations in Eq. (9) are associated, respectively, with $\chi_p^R(x, y)$ and $\chi_p^I(x, y)$ whose control makes it feasible to attain the modulations on $\chi_p^R(x, y)$ and $\chi_p^I(x, y)$ that are "not-in-phase" we sought for. We will discuss the corresponding nontrivial modulations on our atomic lattice in the next section.

III. RESULTS AND DISCUSSION.

Now we examine and discuss the far-field Fraunhofer diffraction that results from driving our 2D atomic lattice both with a (*A.*) $\mathcal{PT}$-symmetry modulation and a (*B.*) hybrid non-Hermitian modulation. We just consider the partial $\mathcal{PT}$ symmetry with respect to the $x \to -x$ and $y \to y$ transformation or the $x \to x$ and $y \to -y$ transformation by plotting the (far-field) diffraction intensity $I_p(\theta_x, \theta_y)$, away from exceptional points and thus immune to secular growths due to spectral singularities [27].

A. $\mathcal{PT}$-symmetry modulation

Our 2D pump cross-grating works in the $\mathcal{PT}$-symmetry regime when $f(x, y)$ is a product of sine functions with $\beta_x = \beta_y = 0$. It is clear that $\chi_p^I(x, y)$ and $\chi_p^R(x, y)$ are spatially out of phase (*i.e.*, differ by $\pi/2$ in phase at each point), with the former (latter) being an odd (even) function along the *four* gray lines in the x and y directions [see Fig. 3(a) and 3(b)]. In addition, $\chi_p^I(x, y)$ exhibits the *double diagonal symmetry* with two positive (negative) peaks in the II and IV (I and III) quadrants in each period of the atomic lattice, while $\chi_p^R(x, y)$ exhibits the *centro symmetry* with a single negative peak centered at the origin. This is further seen by extracting numerical values from the density plots of Fig. 3(a) and 3(b), namely along the $x = y$ [see Fig. 3(c)] and $x = -y$ [see Fig. 3(d)] lines, respectively. The balanced gain for $x = y$ and loss for $x = -y$ (accompanied by the same dispersion) in the 2D $\mathcal{PT}$-symmetry regime can be thought of as the extension of the balanced gain regime for $x > 0$ and loss for $x < -0$ (accompanied by the same dispersion) in the 1D $\mathcal{PT}$-symmetry regime.

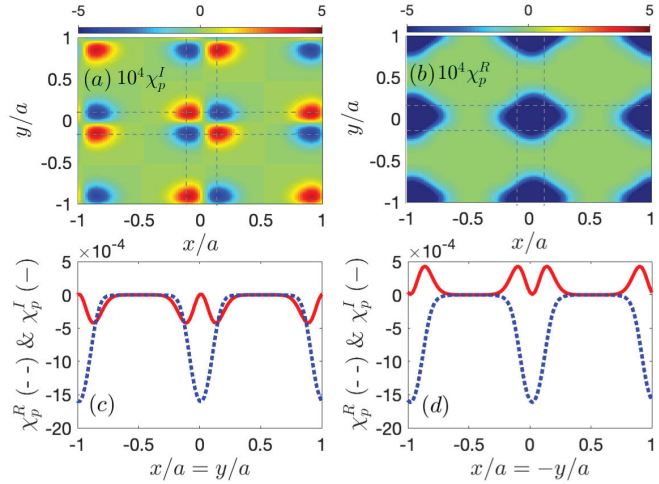

FIG. 3: Absorption (a) and dispersion (b) distributions of a 2D $\mathcal{PT}$-symmetry atomic lattice attained for $\beta_x = \beta_y = 0$, together with their 1D projections along the $x = y$ (c) and $x = -y$ (d) directions. Other parameters are $\Omega_d = 2.0$ MHz, $\Omega_{c0} = 4.5$ MHz, $\delta\Omega_c = 1.6$ MHz, $\delta_p = 5.96$ MHz, $\Delta_c = \Delta_d = 0$, $R = 4$, $M = 10$, $L = 100$ μm, and $N_0 = 3.5 \times 10^{11}$ cm^{-3}.

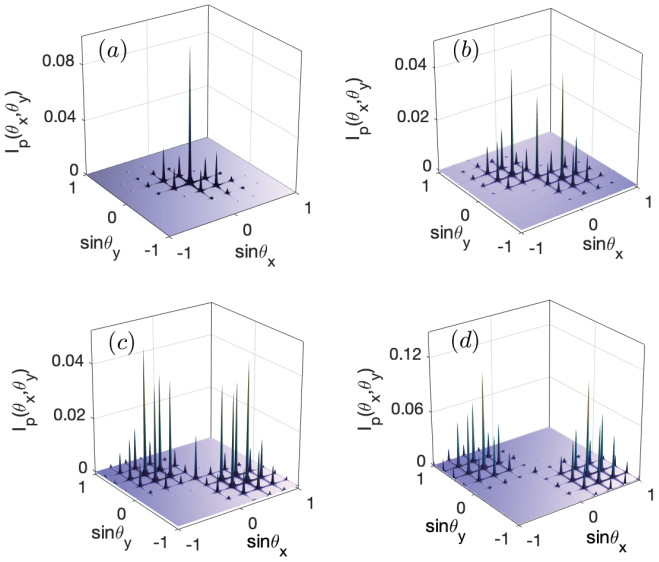

FIG. 4: Diffraction intensity $I_p(\theta_x, \theta_y)$ vs. diffraction angles θ_x and θ_y for a 2D $\mathcal{PT}$-symmetry pump grating. Parameters are as in Fig. 3 except $N_0 = 6.5 \times 10^{11}$ cm^{-3} (a); 8.7×10^{11} cm^{-3} (b); 10.8×10^{11} cm^{-3} (c); 13.0×10^{11} cm^{-3} (d).

Figure 4 reports instead the diffraction intensity distribution for a 2D $\mathcal{PT}$-symmetry pump grating. We observe (i) diffracted photons only in the II and IV quadrants, corresponding to regions where $\chi_p^I(x, y) > 0$ (gain) and $\chi_p^R(x, y) < 0$ (abnormal dispersion) with (ii) the d-

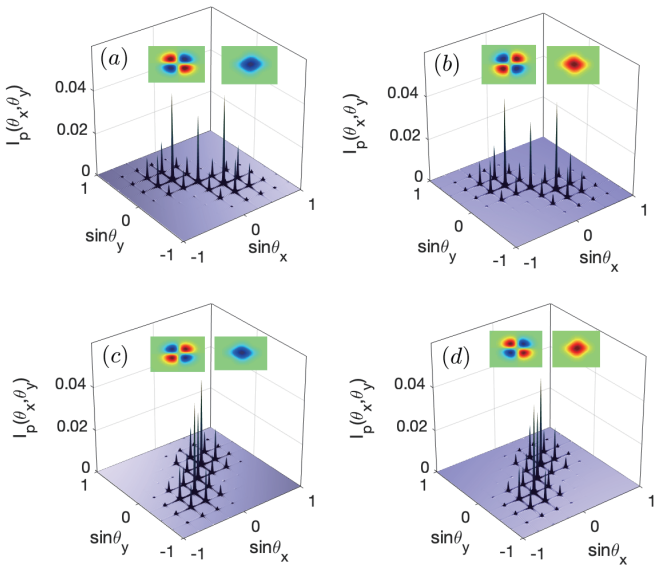

FIG. 5: Diffraction patterns of double diagonal symmetry attained for $\mathcal{PT}$-symmetry modulations along both x and y directions. Parameters are as in Fig. 3(b) except $\delta_p = 5.96$ MHz and $\beta_y = 0$ (a); $\delta_p = -5.96$ MHz and $\beta_y = \pi$ (b); $\delta_p = 5.96$ MHz and $\beta_y = \pi$ (c); $\delta_p = -5.96$ MHz and $\beta_y = 0$ (d). The insets show corresponding absorption (left) and dispersion (right) distributions in a single square lattice.

iffraction pattern largely dependent on N_0, having more photons scattered into higher diffraction orders as N_0 increases. Therefore, 2D $\mathcal{PT}$-symmetry modulations lead to diffraction patterns of *double diagonal symmetry* with respect to the $x = y$ and $x = -y$ lines, being N_0 a crucial parameter to control how probe photons are distributed among different diffraction orders.

Finally we address the question as to whether one may dynamically control "on demand" such an intriguing diffraction pattern. Figure 5 shows that the double diagonal symmetric diffraction, either in the II and IV or in the I and III quadrants, depends on the *signs* of the probe detuning δ_p and the modulating factor $f(x, y)$, the latter being controlled through the shifts β_x and β_y [67]. In particular, if we change the signs of *both* δ_p and $f(x, y)$ from "$+$" to "$-$" the pattern remains bound to the II and IV quadrants, yet when *only* one sign is changed the whole pattern undergoes a $\pi/2$ rotation into the I and III quadrants. Because (i) the simultaneous sign change of δ_p and $f(x, y)$ results in the simultaneous sign change of $\chi_p^I(x, y)$ and $\chi_p^R(x, y)$ and (ii) the sign change of only δ_p or $f(x, y)$ results in the sign change of only $\chi_p^I(x, y)$ or $\chi_p^R(x, y)$, it is clear that the spatial interplay between the amplitude $\propto \chi_p^I(x, y)$ and phase $\propto \chi_p^R(x, y)$ modulations of the transmission $T_L(x, y)$, are responsible for this double diagonal symmetric type of diffraction. We may further conclude from the insets that probe photons are always diffracted into the quadrants where (*1.*) $\chi_p^I(x, y)$ is positive (gain) when $\chi_p^R(x, y)$ is negative (anomalous dispersion) or where (*2.*) $\chi_p^I(x, y)$ is negative (loss) when $\chi_p^R(x, y)$ is positive (normal dispersion).

B. Hybrid non-Hermitian modulation

We now consider two cases when our atomic lattice is driven by the 2D pump cross-grating into a *hybrid* non-Hermitian regime, whereby (*i.*) a $\mathcal{PT}$-symmetry (Hermitian) modulation is applied along the x (y) or y (x) axis; (*ii.*) different non-Hermitian modulations are applied along the x and y axes. A Hermitian modulation along the x axis is attained by setting $\beta_x = \pm\pi/2$, while a non-Hermitian modulation along the x axis is attained by setting $\beta_x = \pm\pi/4$ or $\pm 3\pi/4$ in the modulating factor $f(x, y)$. Similarly when a Hermitian or non-Hermitian modulation along the y axis is sought for.

Figure 6 shows that in case (*i.*) probe photons are diffracted into *adjacent* quadrants, leading to *single axial symmetric* far-field diffraction. In particular, we have observed symmetric (asymmetric) diffraction in quadrants II and III with respect to the x (y) axis for $\beta_x = 0$ and $\beta_y = \pi/2$ [see Fig. 6(a)], quadrants I and IV with respect to the x (y) axis for $\beta_x = 0$ and $\beta_y = -\pi/2$ [see Fig. 6(b)], quadrants III and IV with respect to the y (x) axis for $\beta_y = 0$ and $\beta_x = \pi/2$ [see Fig. 6(c)], and quadrants I and II with respect to the y (x) axis for $\beta_y = 0$ and $\beta_x = -\pi/2$ [see Fig. 6(d)]. We then control the single axial symmetric type of diffraction to realize $\pi/2$-rotations through an appropriate choice of β_x and β_y among the values $\{0; \pm\pi/2\}$. Such a control results into light diffraction symmetric along the direction displaying Hermitian modulation, yet asymmetric along the direction exhibiting $\mathcal{PT}$-symmetry modulation.

Figure 7 shows that in case (*ii.*) probe photons are diffracted into *single quadrants* leading to single diagonal symmetry with respect to the $x = y$ or $x = -y$ line. Control of this diffraction pattern takes place through an appropriate choice of the shifts β_x and β_y among the values $\{\pm\pi/4, \pm 3\pi/4\}$, whereby the modulating factor $f(x, y)$ is neither odd nor even along both x and y axes. Once again, the hybrid non-Hermitian regime, realized via the modulations (*i.*) and (*ii.*) responsible respectively for the single axial symmetry in Fig. 6 and the single diagonal symmetry in Fig. 7 of far-field diffraction, hinges on the spatial interplay between the amplitude $\propto \chi_p^I(x, y)$ and phase $\propto \chi_p^R(x, y)$ modulations of the transmission $T_L(x, y)$; the probe photons are always diffracted into the quadrants where (*1.*) $\chi_p^I(x, y)$ is positive (gain) when $\chi_p^R(x, y)$ is negative or (*2.*) $\chi_p^I(x, y)$ is negative (loss) when $\chi_p^R(x, y)$ is positive as shown by the insets.

The results shown in the last two subsections are finally summed up in Tab. I where the relationship between parameters and types of the 2D cross SW modulations (*A.* and *B.*) and patterns and symmetries of the corresponding far-field Fraunhofer diffraction are sketched. For completeness, we also give the results corresponding to the

TABLE I: **Diffraction patterns and symmetries for four pure or hybrid cross-modulations**

SW pump phases	modulation types	diffraction patterns	diffraction symmetries
$\beta_x = \pi/2$ & $\beta_y = \pi/2$	Hermitian & Hermitian	4 quadrants	centro symmetry
$\beta_x = 0$ & $\beta_y = 0$	$\mathcal{PT}$ symmetry & $\mathcal{PT}$ symmetry	2 diagonal quadrants	double diagonal symmetry
$\beta_x = 0$ & $\beta_y = \pi/2$	$\mathcal{PT}$ symmetry & Hermitian	2 adjacent quadrants	single axial symmetry
$\beta_x = \pi/4$ & $\beta_y = \pi/4$	non-Hermitian & non-Hermitian	1 quadrant	single diagonal symmetry

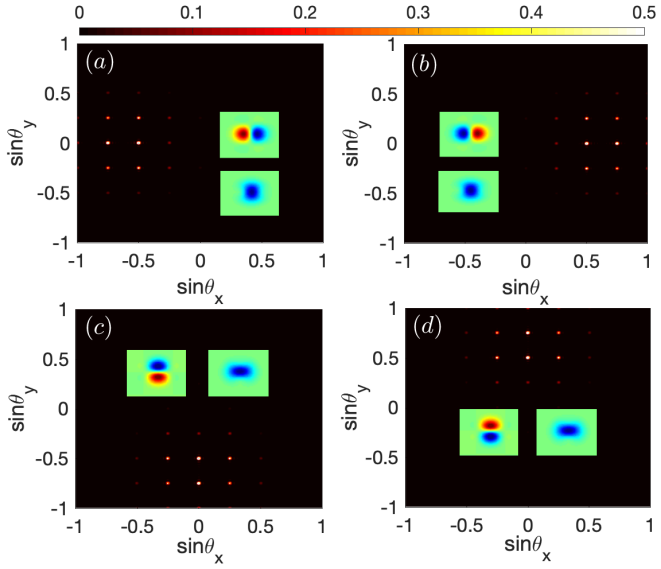

FIG. 6: Diffraction patterns of single axial symmetry attained for a $\mathcal{PT}$-symmetry modulation along the x (or y) direction and a Hermitian modulation along the y (or x) direction. Parameters are as in Fig. 3(b) except that here $\beta_x = 0$ and $\beta_y = \pi/2$ (a); $\beta_x = 0$ and $\beta_y = -\pi/2$ (b); $\beta_y = 0$ and $\beta_x = \pi/2$ (c); $\beta_y = 0$ and $\beta_x = -\pi/2$ (d). The insets show corresponding absorption (upper or left) and dispersion (lower or right) distributions in a single square lattice.

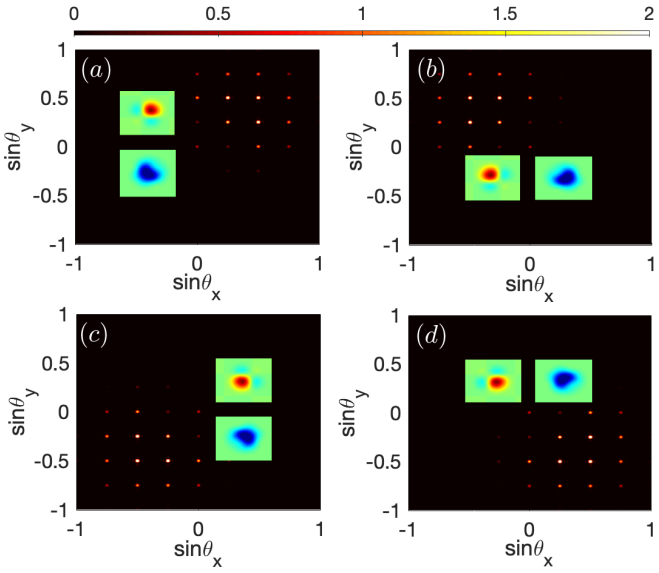

FIG. 7: Diffraction patterns of single diagonal symmetry attained for non-Hermitian modulations along both x and y axes. Parameters are as in Fig. 3(b) except that $\beta_x = \pi/4$ and $\beta_y = \pi/4$ (a); $\beta_x = -\pi/4$ and $\beta_y = -3\pi/4$ (b); $\beta_x = -\pi/4$ and $\beta_y = -\pi/4$ (c); $\beta_y = \pi/4$ and $\beta_y = 3\pi/4$ (d). The insets show corresponding absorption (upper or left) and dispersion (lower or right) distributions in a single square lattice.

normal grating with a Hermitian modulation along both x and y axes ($\beta_x = \beta_y = \pi/2$). In this case, photons can be scattered into all four quadrants with diffraction patterns of the centro symmetry. It is not difficult to imagine that diffraction patterns exhibiting more involved symmetries/asymmetries could be observed upon choosing values for β_x and β_y different from those we have used. On more general grounds, our results are relevant to novel all-optical switching as well as optical imaging even for very weak probe fields. To this extent, as often the case with driven atomic level configurations, it is worth noting that the 2D non-Hermitian cross-gratings investigated here exhibit a certain versatility. In principle, they could be adapted to atom photonic crystal fiber interfaces, dealing even with few-photon light signals [68, 69], or to solid interfaces with rare-earth-ions doped crystals [70, 71] or NV color centers in diamond [72] where similar four-level $\mathcal{N}$ configurations exist.

IV. CONCLUSIONS

The 2D optical lattices of driven cold atoms can provide an interesting venue to realize non-Hermitian EIG structures with novel diffraction symmetry features. We have examined the far-field Fraunhofer diffraction off a thin 2D atomic lattice subject to transversely periodic cross-modulations, including pure $\mathcal{PT}$-symmetry ones as well as hybrid ones as a combination of Hermitian, $\mathcal{PT}$-symmetry, and non-Hermitian modulations along two orthogonal axes. These spatial modulations, now realizable through standard laboratory routines [73], can be all-optically controlled to generate nontrivial far-field patterns that span from double diagonal symmetric diffraction in two diagonal quadrants to single axial symmetric diffraction in two adjacent quadrants and single diagonal symmetric diffraction in a single quadrant. These patterns appear to be fairy robust against standard sources of noises (fluctuations), *e.g.*, in the atomic density or in the intensity of trapping/pumping lasers [74]. The origin of the peculiar diffraction patterns we anticipate is

discussed in terms of the out-of-phase interplay of the amplitude $\propto \chi_p^I(x,y)$ and phase $\propto \chi_p^R(x,y)$ of the transmission $T(x,y)$ through the atomic lattice.

Acknowledgments

This work is supported by the National Natural Science Foundation of China (Nos. 10534002, 11674049, and 11704063); the Cooperative Program by the Italian Ministry of Foreign Affairs and International Cooperation (No. PGR00960) and the National Natural Science Foundation of China (No. 11861131001).

[1] C. M. Bender, Rep. Prog. Phys. **70**, 947 (2007).
[2] R. El-Ganainy, K. G. Makris, D. N. Christodoulides, and Z. H. Musslimani, Opt. Lett. **32**, 2632 (2007).
[3] C. Hang, G. Huang, and V. V. Konotop, Phys. Rev. Lett. 110, 083604 (2013).
[4] J. Sheng, M.-A. Miri, D. N. Christodoulides, and M. Xiao, Phys. Rev. A **88**, 041803(R) (2013).
[5] L. Ge and H. E. Tureci, Phys. Rev. A **88**, 053810 (2013).
[6] J.-H. Wu, M. Artoni, and G. C. La Rocca, Phys. Rev. Lett **113**, 123004 (2014).
[7] J.-H. Wu, M. Artoni, and G. C. La Rocca, Phys. Rev. A **91**, 033811 (2015).
[8] P. Peng, W. Cao, C. Shen, W. Qu, J. Wen, L. Jiang, and Y. Xiao, Nat. Phys. **12**, 1139 (2016).
[9] F. Yang, Y.-C. Liu, and L. You, Phys. Rev. A **96**, 053845 (2017).
[10] X. Wang and J.-H. Wu, Opt. Express **24**, 4289 (2016).
[11] Y. L. Chuang, Ziauddin, and R. K. Lee, Opt. Express **26**, 21969 (2018).
[12] V. V. Konotop and D. A. Zezyulin, Phys. Rev. Lett. **120**, 123902 (2018).
[13] S. Longhi, Phys. Rev. Lett. **103**, 123601 (2009).
[14] Y. Zhang, D. Zhang, Z. Zhang, C. Li, Y. Zhang, F. Li, M. R. Belić, and M. Xiao, Optica **4**, 571 (2017).
[15] Y.-D. Chong, L. Ge, H. Cao, and A. D. Stone, Phys. Rev. Lett. **105**, 053901 (2010).
[16] H. Hodaei, M.-A. Miri, M. Heinrich, D. N. Christodoulides, and M. Khajavikhan, Science **346**, 975 (2014).
[17] L. Feng, Z.-J. Wong, R.-M. Ma, Y. Wang, and X. Zhang, Science **346**, 972 (2014).
[18] B. Peng, Ş. K. Özdemir, S. Rotter, H. Yilmaz, M. Liertzer, F. Monifi, C. M. Bender, F. Nori, and L. Yang, Science **346**, 328 (2014).
[19] H. Jing, Ş. K. Özdemir, X.-Y. Lü, J. Zhang, L. Yang, and F. Nori, Phys. Rev. Lett. **113**, 053604 (2014).
[20] M. Kulishov, J. M. Laniel, Ni. Bélanger, J. Azaña and D. V. Plant, Opt. Express **13**, 3068 (2005).
[21] Z. Lin, H. Ramezani, T. Eichelkraut, T. Kottos, H. Cao, and D. N. Christodoulides, Phys. Rev. Lett. **106**, 213901 (2011).
[22] X. Yin and X. Zhang, Nat. Mater **12**, 175 (2013).
[23] L. Feng, Y.-L. Xu, W. S. Fegadolli, M.-H. Lu, J. E. B. Oliveira, V. R. Almeida, Y.-F. Chen, and A. Scherer, Nat. Mater. **12**, 108 (2013).
[24] M. Kulishov and B. Kress, Opt. Express **20**, 29319 (2012).
[25] M. Kulishov, B. Kress, and H. F. Jones, Opt. Express **22**, 23164 (2014).
[26] M. Kulishov, H. F. Jones, and B. Kress, Opt. Express **23**, 9347 (2015).
[27] S. Longhi, Phys. Rev. A, **81**, 022102 (2010).
[28] M. Fleischhauer, A. Imamoğlu, and J. P. Marangos, Rev. Mod. Phys. **77**, 633 (2005).
[29] K. Hammerer, A. S. Sørensen, and E. S. Polzik, Rev. Mod. Phys. **82**, 1041 (2010).
[30] M. Saffman, T. G. Walker, and K. Mølmer, Rev. Mod. Phys. **82**, 2313 (2010).
[31] A. Imamoğlu, Phys. Rev. Lett. **89**, 163602 (2002).
[32] M. F. Yanik, W. Suh, Z. Wang, and S. Fan, Phys. Rev. Lett. **93**, 233903 (2004).
[33] X. Yang, M. Yu, D.-L. Kwong, and C. W. Wong, Phys. Rev. Lett. **102**, 173902 (2009).
[34] Y. Zou, Y. Jiang, Y. Mei, X. Guo, and S. Du, Phys. Rev. Lett. **119**, 050602 (2017).
[35] A. André and M. D. Lukin, Phys. Rev. Lett. **89**, 143602 (2002).
[36] M. Artoni and G. C. La Rocca, Phys. Rev. Lett. **96**, 073905 (2006).
[37] Y. Zhang, Y.-M. Liu, X.-D. Tian, T.-Y. Zheng, and J.-H. Wu, Phys. Rev. A **91**, 013826 (2015).
[38] M. Bajcsy, A. S. Zibrov, and M. D. Lukin, Nature **426**, 638 (2003).
[39] J.-H. Wu, M. Artoni, and G. C. La Rocca, Phys. Rev. A **82**, 013807 (2010).
[40] J. L. Everett, G. T. Campbell, Y.-W. Cho, P. Vernaz-Gris, D. Higginbottom, O. Pinel, N. P. Robins, P. K. Lam, and B. C. Buchler, Nat. Phys. **13**, 68 (2017).
[41] H.-Y. Ling, Y.-Q. Li, and M. Xiao, Phys. Rev. A **57**, 1338 (1998).
[42] M. Mitsunaga and N. Imoto, Phys. Rev. A **59**, 4773 (1999).
[43] G. C. Cardoso and J. W. R. Tab osa, Phys. Rev. A **65**, 033803 (2002).
[44] L. Zhao, W. Duan, and S. F. Yelin, Phys. Rev. A **82**, 013809 (2010).
[45] M. V. Berry, J. Phys. A **31**, 3943 (1998).
[46] V. V. Konotop and B. I. Mantsyzov, Opt. Express **24**, 26146 (2016).
[47] Y.-M. Liu, X.-D. Tian, X. Wang, D. Yan, and J.-H. Wu, Opt. Lett. **41**, 408 (2016).
[48] S. Asghar, Ziauddin, S. Qamar, and S. Qamar, Phys. Rev. A **94**, 033823 (2016).
[49] Y.-M. Liu, F. Gao, C.-H. Fan, and J.-H. Wu, Opt. Lett. **42**, 4283 (2017).
[50] T. Shui, W.-X. Yang, S. Liu, L. Li, and Z. Zhu, Phys. Rev. A **97**, 033819 (2018).
[51] S.-C. Tian, R.-G. Wan, L.-J. Wang, S.-L. Shu, H.-Y. Lu, X. Zhang, C.-Z. Tong, J.-L. Feng, M. Xiao, and L.-J. Wang, Opt. Express **26**, 32918 (2018).
[52] F. Gao, Y.-M. Liu, X.-D. Tian, C.-L. Cui, and J.-H. Wu, Opt. Express **26**, 33818 (2018).
[53] D.-D. Ma, D.-M. Yu, X.-D. Zhao, and J. Qian, Phys. Rev. A **99**, 033826 (2019).
[54] N.-F. Yu and F. Capasso, Nat. Mater. **13**, 139 (2014).
[55] C. Pfeiffer and A. Grbic, Phys. Rev. Appl. **2**, 044012 (2014).

[56] A. M. Shaltout, V. M. Shalaev, and M. L. Brongersma, Science **364**, 648 (2019).

[57] I. Bloch, Quantum gases in optical lattices, Physics World, Features, (2004).

[58] I. Bloch, Nat. Phys. **1**, 23-30 (2005).

[59] The consideration of other low lying states would not change much our results, yet making the treatment overly complicated. We have checked that our conclusions hold even for a Lorentzian distribution of atomic density.

[60] Here N_0 is basically determined as atoms are preliminarily loaded into a magneto-optical trap. But it is viable to get a higher (lower) N_0 and a smaller (larger) $\sigma_{x,y}$ by ramping up (down) the depth of optical lattice traps.

[61] C. Gardiner and P. Zoller, "Quantum noise: A Handbook of Markovian and Non-Markovian Quantum Stochastic Methods with Applications to Quantum Optics" (2nd enlarged ed., Springer series in synergetics, 2004).

[62] L. Wang, F.-X. Zhou, P.-D. Hu, Y.-P. Niu, and S.-Q. Gong, J. Phys. B: At. Mol. Opt. Phys. **47**, 225501 (2014).

[63] J.-C. Wu and B.-Q. Ai, J. Phys. B: At. Mol. Opt. Phys. **48**, 115504 (2015).

[64] Though one should know, in principle, the full (electric) field inside the grating volume, we assume here that the scattered field be sufficiently small in amplitude and phase as compared to the incident one so that propagation effects could be less relevant. This is clearly an approximation (thin scatterer) to model the field inside and requires that (*i.*) there is only little loss/gain and (*ii.*) the overall phase change is small. The two conditions hold naturally when we notice from Fig. 3 that χ_p^R and χ_p^I have maximal magnitudes on the order of 10^{-3} for an atomic lattice of density $N_0 \sim 10^{12}$ cm^{-3} and length $L = 100$ μm [57, 58].

[65] For the specific driving conditions we examine, the susceptibility in Eq. (2) is sufficiently small so that the associated refractive index $n = \sqrt{1+\chi_p}$ is very close to unity (vacuum value) and hence boundary conditions can be safely neglected in calculating the transmission [66].

[66] M. Artoni, G. C. La Rocca, F. Cataliotti, and F. Bassani, Phys. Rev. A **63**, 023805 (2001).

[67] If one changes, *e.g.*, $\beta_x \to \beta_x + \pi$ or $\beta_y \to \beta_y + \pi$ [see Eq. (6)], then $f(x,y) \to -f(x,y)$.

[68] V. Venkataraman, K. Saha, P. Londero, and A. L. Gaeta, Phys. Rev. Lett. **107**, 193902 (2011).

[69] M. Artoni and R. Loudon, Phys. Rev. A **57**, 622 (1998).

[70] Y.-F. Fan, H.-H. Wang, R. Wang, X.-G. Wei, A.-J. Li, Z.-H. Kang, J.-H. Wu, H.-Z. Zhang, H.-L. Xu, and J.-Y. Gao, New J. Phys. **13**, 123008 (2011).

[71] Q.-Y. He, Y. Xue, M. Artoni, G. C. La Rocca, J.-H. Xu, and J.-Y. Gao, Phys. Rev. B **73**, 195124 (2006).

[72] M. W. Doherty, N. B. Manson, P. Delaney, F. Jelezko, J. Wrachtrup, and L. C. L. Hollenberg, Phys. Rep. **528**, 1 (2013).

[73] Z. Y. Zhang, L. Yang, J. L. Feng, J. T. Sheng, Y. Q. Zhang, Y. P. Zhang, and M. Xiao, Laser. Photon. Rev. **12**, 1800155 (2018).

[74] We have checked that appreciable influences on the 2D diffraction patterns can only be observed for $\sim 5\%$ ($\sim 10\%$) or larger random fluctuatons on N_0 ($\delta\Omega_c$).